Enhanced Oxidation of Nickel at Room Temperature by Low-energy Oxygen Implantation

Robert Peter, Iva Šarić, Mladen Petravić*

Department of Physics and Center for Micro- and Nanosciences and Technologies, University of Rijeka, R. Matejčić 2, HR-51000 Rijeka, Croatia
* Corresponding author's e-mail address: mpetravic@phy.uniri.hr

——— THIS PAPER IS DEDICATED TO PROF. MIRJANA METIKOŠ-HUKOVIĆ ON THE OCCASION OF HER BIRTHDAY ———

Abstract: The formation of oxide films on pure Ni surfaces by low energy oxygen ion-beam bombardment at room temperature was studied by X-ray photoelectron spectroscopy. Ion-induced oxidation is more efficient in creating thin NiO films on Ni surfaces than oxidation in oxygen atmosphere. The oxide thickness of bombarded samples is related to the penetration depth of oxygen ions in Ni and scales with the dose of implanted oxygen, Φ, as $\Phi^{1/6}$. This type of oxide growth is predicted theoretically for diffusion of Ni cations by doubly charged cation vacancies, which creation and mobility is greatly enhanced by ion-irradiation.

Keywords: oxidation of Ni, XPS, ion-beam bombardment, parabolic growth rate, oxygen implantation, NiO, oxidation in oxygen atmosphere.

INTRODUCTION

MOST metal surfaces exposed to an oxidizing environment will gradually corrode. However, many metals, such as chromium, cobalt or nickel, form an inert oxide layer on the surface that isolates the surface from the surrounding environment and provides an effective protection from further deterioration. This phenomenon, called the passivity, is the central issue of the corrosion science[1] with a great relevance in a number of applications, ranging from the heterogeneous catalysis or chemical sensors, to the production of electrochromic devices, transparent conductive films or biomedical devices.[2–6] Nickel is one of the model metals for the oxidation studies as it forms only one oxide, NiO, under wide range of temperatures, T, and oxygen partial pressures, p_{O_2}.[7] Microscopically, the oxidation process in oxygen atmosphere starts with the chemisorption of oxygen at the very top of Ni surface, followed by the nucleation of NiO islands that eventually coalesce, even at room temperature, RT, and form a thin NiO film of several monolayers.[8] This thin NiO film passivates the surface. The further oxide growth requires higher temperatures. As NiO is a metal deficient ($Ni_{1-\delta}O$) p-type semiconductor, the subsequent oxidation of Ni at higher temperatures is expected to proceed by the outward migration of Ni cations and electrons with the growth of a single-phase oxide at the oxide/gas interface.[1] Indeed, the mass transport by diffusion of Ni cations, with a possible contribution from an inward diffusion of oxygen anions, has been identified in a number of oxidation studies of Ni, including the high temperature experiments (500 to 1400 °C),[7,9–12] or oxidation during potentiostatic anodic polarization on pure Ni.[13]

It is very important to gain information on the initial oxidation stage of Ni, as it represents the very first step of Ni reaction with the oxidizing environment. However, at high temperatures, this initial reaction is very fast and it is difficult to determine all aspects of the initial oxidation stages, including the oxidation mechanism. On the other hand, the rapid passivation of Ni surface at RT prevents any further adsorption of oxygen and growth of thicker Ni oxides. In order to study the low-temperature oxidation of Ni, the oxidation chemistry of Ni should be enhanced, not by increasing temperature, but by implementing some other extreme conditions. Indeed, the irradiation of Ni by beams of electrons or Ar+ ions during oxygen exposure enhances significantly the oxidation rate and the formation of Ni oxides.[8,14] In addition, it has been shown that the oxygen implantation represents an attractive and feasible

alternative for oxidation of Ni, even at RT,[15] that could be more efficient in creating thin NiO films on Ni surfaces than oxidation by some other methods, such as electrochemical methods.[16] In addition, the composition and thickness of oxides can be finely controlled, even at RT, simply by tuning the implantation parameters, such as impact angles and energies or doses of implanted oxygen.[15,17–20] In the present study, we explore further the radiation-enhanced oxidation of Ni at RT by the low-energy oxygen ion-beam bombardment in order to examine the oxidation kinetics during initial stages of oxidation process. X-ray photoelectron spectroscopy (XPS) characterization of oxidized surfaces was used in order to compare the initial stages of oxidation of pure Ni metal in oxygen atmosphere at RT with the oxidation of the same material by the oxygen ion-implantation at RT.

EXPERIMENTAL

The oxidation studies were performed on a 0.5 mm-thick nickel foil (Alfa Aesar, 99.994 wt. % Ni). Before any oxidation step, the foil was abraded with SiC papers (800−1200 grit), cleaned with ethanol and redistilled water and then slightly etched within the analysis ultrahigh vacuum (UHV) chamber by cycles of 2 keV Ar$^+$ bombardment at RT (these samples are referred to as cleaned samples). The cleaned samples were oxidised *in situ* in oxygen atmosphere, under the pure oxygen-gas (purity 99.999 %) pressures around 2×10^{-4} Pa. The oxidation dose is expressed in units of Langmuir, connected to the gas pressure (in Pa) and the exposure time (in seconds) as 1 L = 1.33×10^{-4} Pa s. The ion-beam oxidation was also carried out *in situ* with a broad beam of 1 or 2 keV O$_2^+$ ions with the typical current density of 2 µA/cm². The implanted dose Φ (in O atoms/cm²) for the conditions used in the present study is related to the bombardment time (t, in seconds), as $1.25 \times 10^{13} \times t$. For the bombardment times used in this study (from 2 seconds to 4 hours), the corresponding implanted dose of oxygen covers almost four orders of magnitude, from 2.5×10^{13} O atoms/cm² to 1.75×10^{17} O atoms/cm².

All samples were characterized by XPS in a SPECS XPS spectrometer equipped with a Phoibos MCD 100 electron analyser and a monochromatized source of Al K$_\alpha$ X-rays of 1486.74 eV. The typical pressure in the UHV chamber during analysis was in the 10^{-7} Pa range. For the electron pass energy of the hemispherical electron energy analyser of 10 eV used in the present study, the overall energy resolution was around 0.8 eV. All spectra were calibrated by the position of C 1*s* peak, placed at binding energy of 284.5 eV. The photoemission spectra were simulated with several sets of mixed Gaussian-Lorentzian functions with Shirley background subtraction.

RESULTS AND DISCUSSION

The development of Ni-O bonds during different oxidation stages on Ni surfaces can be obtained from the chemical shifts in photoemission spectra around the Ni 2*p* or O 1*s* core levels. While the focus of XPS measurements in the present study was on the Ni 2*p* photoemission that shows the more distinctive structure and larger chemical shifts than the O 1*s* emission,[21] the O 1*s* photoemission was also monitored in order to follow up the build-up of oxygen concentration in the near surface region during each oxidation step. The Ni 2*p* emission is characterized by two asymmetric peaks at binding energies, BE, of 852.5 eV and 869.9 eV, respectively, characteristic for the spin-orbit splitting of the Ni 2*p* energy level of metallic Ni, Ni(0), into 2*p*$_{3/2}$ and 2*p*$_{1/2}$ levels, respectively (not shown).[22] In the present work we have considered only the more intense Ni 2*p*$_{3/2}$ component, as the large Ni 2*p* spin-orbit splitting of around 17 eV prevents any mixing of contributions from 2*p*$_{3/2}$ and 2*p*$_{1/2}$ states.[21]

Several characteristic Ni 2*p*$_{3/2}$ spectra obtained from cleaned and oxidized Ni surfaces are shown in Figure 1. The photoemission from a cleaned sample is characterized by the metallic Ni(0) peak (peak 1 at BE of 852.5 eV) and a less intensive satellite peak (peak 1' at BE around 858.5 eV; the fitting of the Ni 2*p*$_{3/2}$ line from the cleaned sample, shown in Figure 2, reveals the second characteristic satellite at BE
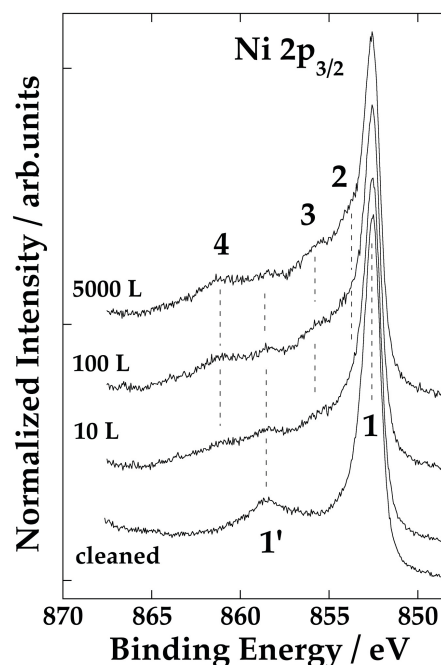

Figure 1. Ni 2*p*$_{3/2}$ core-level photoemission spectra from a cleaned nickel surface and surfaces oxidized at RT in oxygen atmosphere to 10, 100 and 5000 L, respectively.

around 586.0 eV, as reported previously in the literature for pure Ni surfaces).[21] After the oxidation in oxygen atmosphere at RT several new peaks emerge in spectra (peaks 2–4 in Figure 1), already after the lowest dose of 10 L of oxygen used in the present study. Intensities of these new peaks increase only slightly for higher oxygen doses, and saturate after around 100 L of oxygen. Obviously, the metallic Ni surface is quite resistant to the oxidation in oxygen atmosphere at RT. The photoemission results from Figure 1 indicate the fast formation of only several monolayers of Ni oxide on the surface of Ni metal that reduces the reactivity of surface and prevents any further adsorption or uptake of oxygen at higher oxygen doses. The further growth of oxide films on Ni requires oxidation temperatures well above RT.

The ion-induced oxidation of Ni induces several dramatic changes in the shape of Ni 2p photoemission peaks, as shown, as an example, in Figure 2 for bombardment of Ni surfaces with 2 keV O_2^+ ions for 300 and 3600 s, respectively (corresponding to Φ of 3.75×10^{15} and 4.5×10^{16} O atoms/cm^2, respectively). The ion-bombarded spectra are fitted with several mixed Gaussian-Lorentzian functions 2–6 (in addition to the metallic, Ni(0), peak 1 and two satellites, 1' and 1'', from the cleaned sample): peak 2 at BE of 853.8 eV, peak 3 at 855.5 eV, and satellite peaks 4, 5 and 6 at 860.7, 863.9 eV and 866.2 eV, respectively. Indeed, the
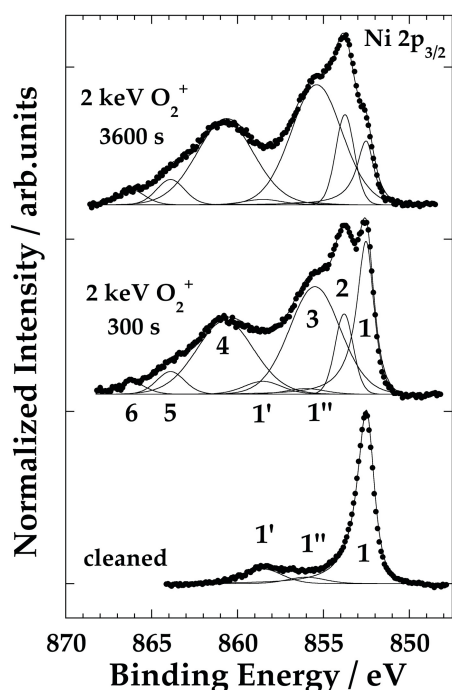
new peaks 2–6 are known from the literature as the characteristic photoemission features from NiO surfaces.[23] A strong metallic Ni(0) peak 1, still present in the spectra after oxidation with the highest oxygen dose used in the present study, indicates the formation of a very thin oxide film on the surface. In such case, the XPS signal includes a contribution from the underlying metallic nickel.

We supplement Ni 2p core-level measurements from Figures 1 and 2 with the XPS measurements around O 1s levels (Figure 3) and the valence band photoemission measurements (Figure 4, obtained also with Al K$_\alpha$ X-rays), respectively. Several characteristic spectra are shown in Figures 3 and 4, respectively. All O 1s spectra in Figure 3 exhibit an intensive peak at 529.5 eV, characteristic for the emission from the O^{2-} states in the transition metal oxides, such as NiO.[24] The smaller peak around 531.3 eV has been assigned previously to the defective oxide (oxygen atoms attached to the lattice vacancies) and/or CO or OH impurities adsorbed on the surface.[21] However, in the case of Ni oxides, this peak has also been assigned to the emission from the Ni$_2$O$_3$ phase that can be present at low concentration within the NiO films.[25] A possible contribution from a Ni$_2$O$_3$ phase in the Ni 2$p_{3/2}$ spectrum is difficult to distinguish within the signal dominated with NiO phase, as the BE of Ni–O bonds in Ni$_2$O$_3$ overlap with the multiplet splitting structure of NiO (peak 3 from Figure 2).[15,26] Although in the present paper we only discuss the formation of a NiO phase, the presence of a small concentration of Ni$_2$O$_3$ phase should also be anticipated within the total concentration of Ni oxide.[15]

Figure 2. Fitting of Ni 2$p_{3/2}$ photoemission peaks, obtained from a cleaned surface and surfaces ion-beam bombarded at RT with 2 keV O_2^+ for 300 and 3600 s. Closed circles represent experimental data and solid lines a mixture of Gaussians and Lorentzians.
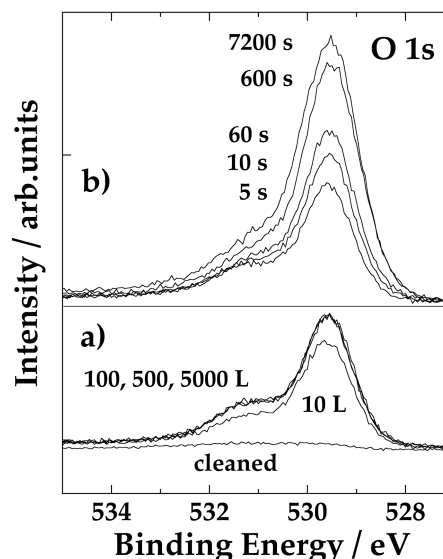
Figure 3. XPS spectra around O 1s core-level measured a) on a cleaned Ni sample and samples oxidized at RT in oxygen atmosphere to different oxygen doses or b) on samples bombarded at RT with 2 keV O_2^+ ions for different times, as indicated in the figure.
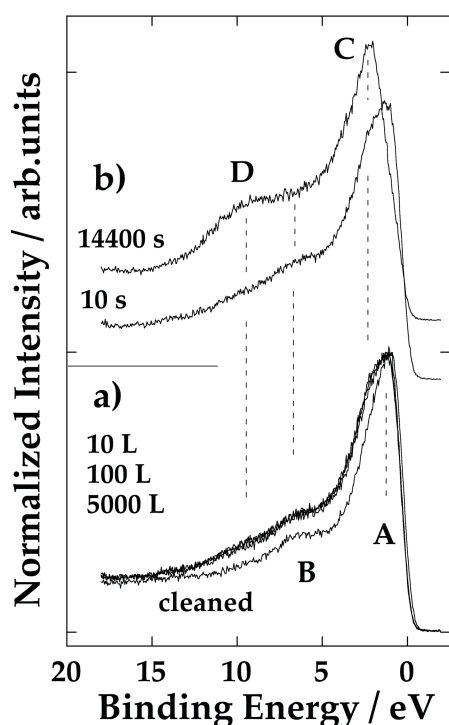
Figure 4. Valence band photoemission spectra (obtained with Al K_α X-rays) from a cleaned Ni surface and surfaces oxidized at RT in oxygen atmosphere to 10, 100 and 5000 L or ion-beam bombarded at RT with 2 keV O_2^+ ions for 10 and 14400 s.

In the case of oxidation in oxygen atmosphere (Figure 3a), the O 1*s* emission increases after exposing the surface to 10 L of oxygen, but remains almost constant for the higher oxygen doses, revealing the saturation of oxygen uptake after the lowest oxygen dose of 10 L. On the other hand, the concentration of oxygen increases continuously with the bombardment time during the ion-implantation experiments (Figure 3b), indicating the continuous build-up of oxygen concentration below the surface. The valence band spectra in Figure 4 exhibit the same trend. The valence band of samples oxidised in oxygen atmosphere (Figure 4a) saturates immediately after the lowest oxygen dose of 10 L. It is characterized by the broadening of peak A, *i.e.* development of an additional peak, C, corresponding to Ni 3d states in NiO.[27,28] In contrast to the oxidation in oxygen atmosphere, the valence band of ion-beam bombarded samples (Figure 4b) exhibits a more complex structure, characteristic for NiO: a well pronounced new peak, C, about 2.2 eV below the Fermi level, corresponding to Ni 3*d* states, and a strong peak D, about 9.5 eV below the Fermi level, representing Ni 3*d* valence band satellites.[27,28]

In general, at low temperatures, the oxidation of Ni in oxygen atmosphere involves the tunnelling of electrons from Ni atoms to the adsorbed O atoms at the surface that produces an electric field across the oxide. This electric field causes the outward migration of metal cations to the surface, or the inward migration of oxygen anions to the oxide/metal interface, resulting in the thickening of the oxide film with the exposure time, best described by a logarithmic growth rate.[29,30] In this process oxidation is terminated when the electric field is no longer strong enough to support the ion migration. However, our oxidation in oxygen atmosphere, carried out at RT, are not consistent with the logarithmic kinetics. The oxidation process saturates very fast and prevents any further oxide growth. It is consistent with the first few steps in the oxidation process described by the dissociation of oxygen molecules from the gas phase and adsorption of separate oxygen atoms on the surface of Ni. As the adsorbed oxygen atoms exchange places with the underlying metal atoms and become incorporated below the surface, a thin oxide layer or oxidized islands form on Ni surface.[8] On the other hand, the oxidation of Ni in oxygen atmosphere at elevated temperatures is driven by Ni^{2+} diffusion through the oxide film. Ni^{2+} cations diffuse through lattice defect sites (such as vacancies created within the oxide) to the surface where they react with adsorbed oxygen, following the parabolic rate law.[9–12] When a Ni vacancy is created, two neighbouring Ni^{2+} atoms, in order to balance charges, each lose an electron forming two Ni^{3+} ions (*i.e.* two electron holes).[1] The incorporation of oxygen in Ni is described by reactions[1]

$$\tfrac{1}{2}\,O_2 \rightarrow O_o^x + V''_{Ni} + 2h^\bullet \;\; ; \;\; \tfrac{1}{2}\,O_2 \rightarrow O_o^x + V'_{Ni} + h^\bullet \qquad (1)$$
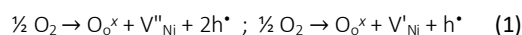
where, in the Kröger-Vink notation, O_o^x represents an O ion on a regular lattice site, V''_{Ni} (V'_{Ni}) is a doubly (singly) ionized Ni vacancy and $h^\bullet$ is a positively charged electron hole. It has been shown (both theoretically and experimentally) that the concentration of cation vacancies scales with the oxygen partial pressure, p_{O_2}, as $(p_{O_2})^n$, where the exponent n equals 1/2, 1/4 or 1/6 for the neutral or singly and doubly charged Ni vacancies, respectively.[1,31,32] Consequently, any quantity, x, directly related to the diffusion of charged particles by cation vacancies within the oxide film, such as the oxide thickness or the change in weight as a result of oxidation, should be related to the oxidation time, t, as $x = K t^n$, *i.e.* $\log(x) = \log(K) + n\log(t)$, where K is the rate constant[1]. Therefore, if the plot of experimental data on a $\log(x)$ *vs.* $\log(t)$ scale produces a straight line, the slope of this line is determined by the exponent n.

The change of thickness, d, of a NiO film with the bombardment time (*i.e.* the oxygen dose Φ) can be determined from the numerical fits of Ni 2*p* photoemission peaks shown in Figure 2. The intensity ratio, $I_{Ni}/I_{Ni\infty}$, of metallic Ni $2p_{3/2}$ peaks (such as peaks 1 in Figure 2), taken from the Ni foil with an oxide film (I_{Ni}) and from a cleaned Ni surface ($I_{Ni\infty}$), is given by the relation[33]

$$I_{Ni} = I_{Ni\infty} \exp[-d/(\lambda \cos \theta)] \qquad (2)$$

where *I* is the area under the metal peak (peak 1 in Figure 2), λ is the inelastic mean free path of electrons ($\lambda = 1.1$ nm for 630 eV electrons from the present XPS measurements[34]) and θ is the emission angle with respect to the surface normal (equals 0° in the XPS instrument used in the present study). The results are plotted on a log(*d*) *vs.* log(*t*) scale in Figure 5 for the two oxygen-ion impact energies of 1 and 2 keV. The saturation oxide thickness obtained by this method is about 2.4 nm for 1 keV O_2^+ ions, while it approaches 3.3 nm for 2 keV oxygen ions. For the comparison, the saturation oxide thickness, obtained from relation (2) for a sample oxidised in oxygen atmosphere at RT to a dose of 5000 L (the largest oxygen dose used in our experiments) is about 0.9 nm. On the other hand, the oxide thickness on ion-bombarded samples can be estimated from SRIM simulations.[35] For 1 keV (or 2 keV) O_2^+ bombardment the ion range (R_p) of oxygen in Ni or NiO changes only slightly from 1.1 to 1.2 nm (or 1.6 to 1.9 nm), while the range straggling (ΔR_p) changes from 0.9 to 1.3 nm (or 1.3 to 1.6 nm) Therefore, the total oxide thickness ($R_p + \Delta R_p$) of 2.0 to 2.5 nm (or 2.9 to 3.5 nm) is expected for 1 keV (or 2 keV) O_2^+ bombardment, in very good agreement with the saturation oxide thickness obtained from XPS measurements plotted in Figure 5.

Several different slopes, also plotted in Figure 5, are related to the mass transport during the oxidation processes driven by the diffusion of cation vacancies of different charge states, as predicted by the theory of parabolic oxidation growth rate.[1] For both ion-bombardment energies (1 or 2 keV) the oxide thickness closely follows the parabolic growth rate with the exponent *n* of about 1/6. This result strongly points to the dominant contribution of doubly charged Ni vacancies, V''_{Ni}, in the mass transport during ion-induced oxidation of pure Ni. It is worth mentioning here that the oxidation of Ni in oxygen atmosphere at elevated temperatures exhibits several different growth rates of NiO, depending on the oxidation temperature. For example, the mass transport estimated from the diffusion coefficients of Ni in NiO as a function of p_{O_2} indicates the $(p_{O_2})^{1/3.5}$ dependence at 1400 °C, $(p_{O_2})^{1/4}$ dependence at 1300 °C and finally a $(p_{O_2})^{1/6}$ dependence bellow 1000 °C.[10] This result confirms the important role of V_{Ni} in mass transport during the thermal oxidation of pure Ni, with a dominant contribution of doubly charged vacancies at 1000 °C and singly charged vacancies at 1300 °C, while neutral vacancies may exist at higher temperatures. In contrast to thermal processes, the ion-induced oxidation eliminates the need for elevated temperatures and bypasses several thermally activated processes, such as absorption, dissociation, place-exchange, diffusion or bond braking, while, at the same time, enhances the production of point defects, such as vacancies and interstitials.[36] The point defects may considerably enhance mobility and reactivity of metal
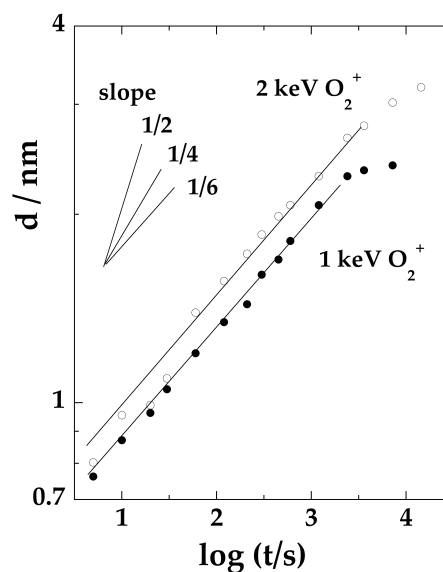

Figure 5. Thickness of oxide films obtained on pure Ni samples by 1 or 2 keV O_2^+ ion-beam bombardment at RT as a function of bombardment time, plotted on a log-log scale. Symbols represent experimental results. Several different slopes, characteristic for different parabolic growth rates, are also indicated in the figure.

cations and oxygen anions in material and, therefore, influence the oxidation process. On the other hand, the sputtering process present during ion-bombardment can limit the final oxide thickness. However, the sputtering rate in our experiments is quite low, at least two orders of magnitude lower than in some other techniques based on sputtering process, such as Secondary ion mass spectrometry (SIMS).[37] From our SIMS measurements on Ni[15], we estimate the sputtering rate in present oxidation experiments to the order of 10^{-3} Å/s. But, more importantly, the oxygen ions are implanted deeper below the surface with an increase of R_p directly related to the erosion rate of the surface by sputtering. For a steady state condition between the sputter-erosion of the surface and the implantation depth of O atoms, the thickness of the final oxide layer does not depend on the sputtering rate.

CONCLUSION

In summary, we present the XPS analysis of the oxidation process on pure Ni surfaces by low-energy oxygen bombardment at RT. The oxidation starts below the surface, at depths within the $R_p + \Delta R_p$ range. Oxygen in excess to the amount consumed in the formation of a shallow buried nickel oxide rapidly diffuses toward the buried oxide interface where it oxidizes the available nickel. At the same time, the outward diffusion of Ni ions through cation

vacancies, created within the buried NiO (the formation of vacancies is further enhanced by ion-bombardment), places more Ni ions close to the surface where they react with the impinging oxygen ions and provide the oxide growth at the oxide/gas interface. This oxidation step is characterized by the parabolic growth rate, which scales with the amount of implanted oxygen as $\Phi^{1/6}$, in contrast to the oxidation processes carried out in an oxygen atmosphere, but in full agreement with the theoretical prediction for the oxidation driven by the diffusion of cations through doubly charged cation vacancies. The oxide thickness is related to the implantation kinetics of oxygen ions and is limited by the simultaneous sputtering of the Ni surface by energetic ion bombardment.

REFERENCES

[1]   D. Young, *High Temperature Oxidation and Corrosion of Metals*, Elsevier, Amsterdam, **2008**.

[2]   B. M. Weckhuysen, D. E. Keller, *Catal. Today* **2003**, *78*, 25.

[3]   I. Hotovy, J. Huran, P. Siciliano, S. Capone, L. Spiess, V. Rehacek, *Sens. Actuators B* **2001**, *78*, 126.

[4]   H. Liu, W. Zheng, X. Yan, B. Feng, *J. Alloys Compd.* **2008**, *462*, 356.

[5]   H. Sato, T. Minami, S. Takata, T. Yamada, *Thin Solid Films* **1993**, *236*, 27.

[6]   Y. Huang, J. F. Kong, S. S. Venkatraman, *Acta Biomater.* **2014**, *10*, 1088.

[7]   G. J. Koel, P. J. Gellings, *Oxid. Met.* **1972**, *5*, 185.

[8]   J. C. de Jestis, P. Pereira, J. Carrazza, F. Zaera, *Surf. Sci.* **1996**, *369*, 217.

[9]   A. Atkinson, D. W. Smart, *J. Electrochem. Soc.* **1988**, *135*, 2886.

[10] K. Fueki, J. B. Wagner, *J. Electrochem. Soc.* **1965**, *112*, 384.

[11] A. Kursumovic, R. Tomov, R. Hühne, B. A. Glowacki, J. E. Everts, A. Tuissi, E. Villa, B. Holzapfel, *Physica C* **2003**, *385*, 337.

[12] S. Chevalier, F. Desserrey, J. P. Larpin, *Oxid. Met.* **2005**, *64*, 219.

[13] J. Katić, M. Metikoš-Huković, I. Milošev, *J. Electrochem. Soc.* **2015**, *162*, C767.

[14] W. Li, M. J. Stirniman, S. J. Sibener, *Surf. Sci.* **1995**, *329*, L593.

[15] I. Saric, R. Peter, I. Kavre, I. Jelovica Badovinac, M. Petravić, *Nucl. Instr. Meth. Phys. Res. B* **2016**, *371*, 286.

[16] J. Katić, M. Metikoš-Huković, R. Peter, M. Petravić, *J. Power Sources* **2015**, *282*, 421.

[17] K. S. Kim, N. Winograd, *Surf. Sci.* **1974**, *43*, 625.

[18] N. V. Alov, *Nucl. Instr. Meth. Phys. Res. B.* **2007**, *256*, 337.

[19] D. L. López-Carreño, G. Benítez, L. Viscido, J. M. Heras, F. Yubero, J. P. Espinós, A. R. González-Elipe, *Surf. Sci.* **1998**, *402*, 174.

[20] I. Saric, R. Peter, M. Petravic, *J. Phys. Chem. C* **2016**, *120*, 22421.

[21] M. C. Biesinger, B. P. Payne, A. P. Grosvenor, W. M. Laua, A. R. Gerson, R. St.C. Smart, *Appl. Surf. Sci.* **2011**, *257*, 2717.

[22] C. D. Wagner, W. Riggs, L. Davis, J. Moulder, *Handbook of X-ray Photoelectron Spectroscopy*, edited by G. E. Muilenberg, Perkin Elmer, Eden Prairie, MN, **1979**.

[23] M. C. Biesinger, B. P. Payne, L. W. M. Lau, A. R. Gerson, R. St.C. Smart, *Surf. Interface Anal.* **2009**, *41*, 324.

[24] B. P. Payne, M. C. Biesinger, N. S. McIntyre, *J. Electron Spectrosc. Relat. Phenom.* **2011**, *184*, 29.

[25] F. S.-S. Chien, Y. T. Wu, G. L. Lai, Y. H. Lai, *Appl. Phys. Lett.* **2011**, *98*, 153513.

[26] D. S. Kim, H. C. Lee, *J. Appl. Phys.* **2012**, *112*, 034504.

[27] M. Taguchi, M. Matsunami, Y. Ishida, R. Eguchi, A. Chainani, Y. Takata, M. Yabashi, K. Tamasaku, Y. Nishino, T. Ishikawa, Y. Senba, H. Ohashi, S. Shin, *Phys. Rev. Lett.* **2008**, *100*, 206401.

[28] J. Das, K. S. R. Menon, *J. Electron Spectrosc. Relat. Phenom.* **2015**, *203*, 71.

[29] N. Cabrera, N. F. Mott, *Rep. Prog. Phys.* **1949**, *12*, 163.

[30] F. P. Fehlner, N. F. Mott, *Oxid. Met.* **1970**, *2*, 59.

[31] C. Wagner, *Z. Phys. Chem. B* **1933**, *21*, 25.

[32] Y. Unutulmazsoy, R. Merkle, D. Fischer, J. Mannhart, J. Maier, *Phys. Chem. Chem. Phys.* **2017**, *19*, 9045.

[33] J. F. Watts, J. Wolstenholme, *An Introduction to surface analysis by XPS and AES*, Wiley, Chichester, **2003**.

[34] S. Tanuma, C. J. Powell, D. R. Penn, *Surf. Interface Anal.* **2010**, *43*, 689.

[35] J. F. Zigler, J. P. Biersack, U. Littmark, *The Stopping and Range of Ions in Solids*, Pergamon, New York, **1986**.

[36] J. S. Williams, J. M. Poate, *Ion implantation and beam processing*, Academic Press, Sydney, **1984**.

[37] R. G. Wilson, F. A. Stevie, C. W. Magee, *Secondary Ion Mass Spectrometry: A Practical Handbook for Depth Profiling and Bulk Impurity Analysis*, John Wiley & Sons, USA, **1989**.